Journal of Solid State Chemistry 182 (2009) 1396–1400

Contents lists available at ScienceDirect

Journal of Solid State Chemistry

journal homepage: www.elsevier.com/locate/jssc

Solvothermal synthesis and photoluminescence properties of $BiPO_4$ nano-cocoons and nanorods with different phases

Fei Xue, Haibo Li, Yongchun Zhu, Shenglin Xiong, Xianwen Zhang, Tingting Wang, Xin Liang, Yitai Qian *

Hefei National Laboratory for Physical Science at Microscale and Department of Chemistry, University of Science and Technology of China, Hefei, Anhui 230026, People's Republic of China

ARTICLE INFO

Article history:
Received 9 December 2008
Received in revised form
14 February 2009
Accepted 27 February 2009
Available online 6 March 2009

Keywords:
$BiPO_4$
Nano-cocoons
Nanorods
Evolution
Photoluminescence

ABSTRACT

Hexagonal phase $BiPO_4$ nano-cocoons and monoclinic phase $BiPO_4$ nanorods have been synthesized in the mixed solvents of glycerol and distilled water with the volume ratio of 2:1 at 200 °C. The solvothermal evolution process from hexagonal phase $BiPO_4$ nano-cocoons to monoclinic phase $BiPO_4$ nanorods was observed by varying the reaction time from 1 to 3 h. In the hydrothermal condition at 160 °C, the similar phase transformation from hexagonal phase $BiPO_4$ to monoclinic phase $BiPO_4$ was also observed, accompanying with a morphology transformation from nanorods to octahedron-like microcrystals. It was found that the volume ratio of glycerol to water in the solvothermal condition had a great impact on the shapes of products, while it had no influence on the formation of different phases. The fluorescence spectra of hexagonal phase $BiPO_4$ nano-cocoons and monoclinic phase $BiPO_4$ nanorods were also studied.

1. Introduction

Bismuth phosphate ($BiPO_4$) was reported to have special applications in catalysis [1,2], ion sensing [3] and separating radioactive elements [4–6], and improving the electric properties of phosphate glasses [7,8]. Recently, it was also reported that $BiPO_4$ exhibited photoluminescence properties [9]. Up to the present, several methods were used to synthesize single-phase $BiPO_4$ micro and nanomaterials. Hexagonal phase $BiPO_4$ nanorods [10] were prepared via a sonochemical method in a surfactant/ligand-free system under ambient air at room temperature. Monoclinic phase $BiPO_4$ nanowires [11] were synthesized by a chemical vapor deposition process. Monoclinic phase $BiPO_4$ urchin-like architectures [9] were formed by a hydrothermal method. Though great progress has been made in preparing $BiPO_4$ nanostructures, preparation of $BiPO_4$ nanocrystals with controlled morphology and phase by a simple route such as variation of the reaction time remains a challenge to material scientists.

In this paper, we describe a controlled solvothermal synthesis of hexagonal phase $BiPO_4$ nano-cocoons and monoclinic nanorods by easily varying reaction time. The phase and morphology evolution from the initially formed hexagonal phase nano-cocoons to monoclinic phase $BiPO_4$ nanorods were investigated by studying intermediate products of different reaction time. The similar phase transformation from hexagonal phase $BiPO_4$ to monoclinic phase $BiPO_4$ in the hydrothermal condition at 160 °C was also observed, accompanying with a morphology transformation from nanorods to octahedron-like microcrystals. Moreover, we found that the volume ratio of glycerol and water had a great impact on the shapes of finial products. Experimental results revealed that $BiPO_4$ nanostructures exhibited photoluminescence properties.

2. Experimental section

2.1. Synthesis of $BiPO_4$ nanostructures

All the reagents were of analytical grade and were used without further purification. In a typical procedure, 1 mmol of $Bi(NO_3)_3 \cdot 5H_2O$ was added to 45 mL glycerol/distilled water mixed-solvent (the volume ratio is 2:1) under magnetic stirring. And then 1 mmol of $NaH_2PO_4 \cdot 2H_2O$ was added to the mixture and the stirring was continued for 1 h. Finally, the mixture was transferred into a Teflon-lined autoclave and the autoclave was sealed and maintained at 200 °C for 1–3 h. The final product was collected, washed with distilled water and absolute alcohol, and then dried at 60 °C for 6 h. The yield of $BiPO_4$ is about 90%.

2.2. Characterizations

The phase identification of the products was accomplished by using powder X-ray diffraction (XRD) employing a Philips X'pert

* Corresponding author. Fax: +86 551 360 7402.
E-mail address: ytqian@ustc.edu.cn (Y. Qian).

0022-4596/$ - see front matter © 2009 Elsevier Inc. All rights reserved.
doi:10.1016/j.jssc.2009.02.031

X-ray diffractometer with Cu$K\alpha$ radiation ($\lambda = 1.54178$ Å). A scan rate of 0.05° s^{-1} was applied to record the pattern in the 2θ range of 10°–60°. FTIR spectra were measured using a Bruker Vector-22 FTIR spectrometer from 4000 to 400 cm^{-1} at room temperature. The transmission electron microscopy (TEM) images were taken with a Hitachi model H-800 transmission electron microscope. The scanning electron microscopy (SEM) images were taken by using a JEOL-JSM-6700F field-emitting (FE) scanning electron microscope. High-resolution (HR) TEM images, selected-area electron diffraction (SAED) and an energy-dispersive X-ray (EDX) spectrum were taken with a JEOL-2010 transmission electron microscope with an accelerating voltage of 200 kV. The fluorescence of the products was determined by a Hitachi 850-luminescence spectrophotometer with a Xe lamp at room temperature.

3. Results and discussion

3.1. XRD patterns of the products

Fig. 1 shows the XRD patterns of products synthesized at 200 °C for 1 and 3 h. When the reaction time was 1 h, all the diffraction peaks in the XRD pattern (Fig. 1a1) of the resulting product can be indexed to the hexagonal phase (JCPDS Cards 45-1370) with lattice constants of $a = 6.986$ Å and $c = 6.475$ Å. When the solvothermal dwell time was extended to 3 h; however, all the diffraction peaks (Fig. 1a2) of the product can be indexed to

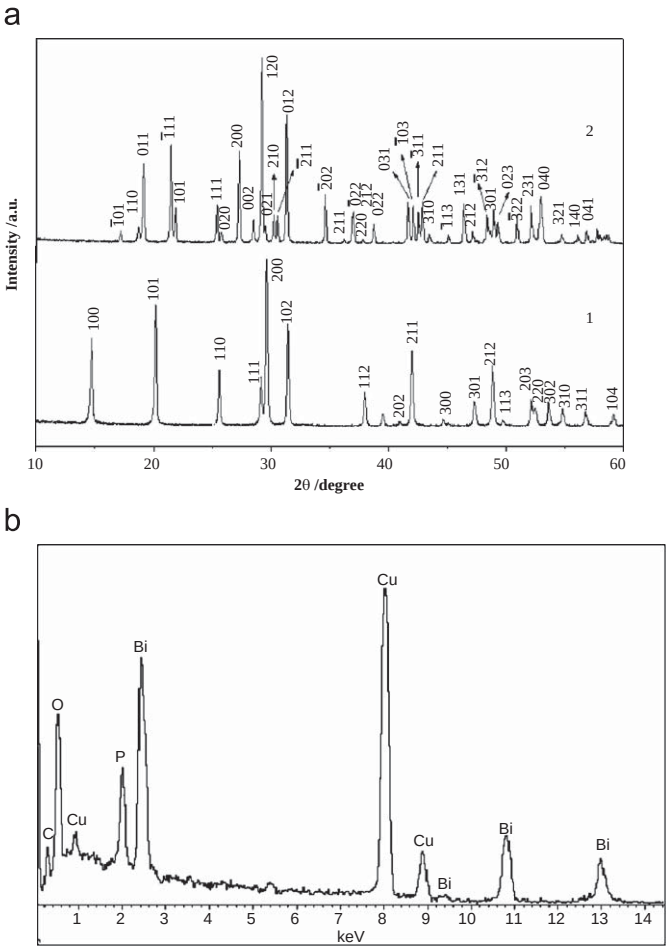

Fig. 1. XRD patterns of (a1) hexagonal $BiPO_4$ prepared at 200 °C for 1 h, (a2) monoclinic $BiPO_4$ at 200 °C for 3 h and (b) EDX spectrum of $BiPO_4$.

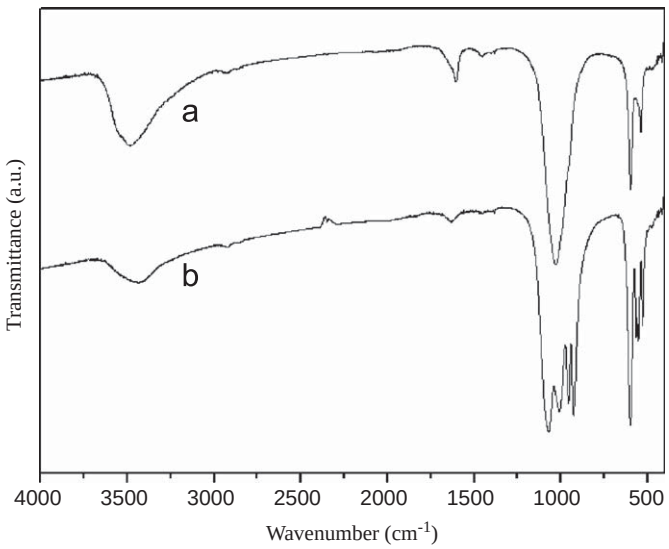

Fig. 2. FTIR spectra of the $BiPO_4$ prepared at 200 °C with different phase: (a) hexagonal phase; (b) monoclinic phase.

the monoclinic phase (JCPDS Cards 80-0209) with lattice constants of $a = 6.762$ Å, $b = 6.951$ Å and $c = 6.482$ Å. No characteristic peak is observed for other impurities. These results show that polymorphic form of $BiPO_4$ can be selectively controlled by varying the reaction time. EDX analysis was also employed to determine the chemical composition. Besides Cu element, only bismuth, phosphorus and oxygen elements were detected with a molar ratio of about 1:1:4 (Bi:P:O). The Cu element in the EDS (Fig. 1b) originates from the copper wafer to support the sample.

3.2. FTIR spectra of the products

Fig. 2a shows the FTIR spectrum of the as-synthesized hexagonal phase $BiPO_4$. The very intense band centered at 1023 cm^{-1} is due to the v_3 stretching vibration of the PO_4 group [12]. The bands centered at 600 and 535 cm^{-1} are assigned to δ (O–P–O) and v_4 (PO_4), respectively [12]. The FTIR spectrum of the monoclinic phase $BiPO_4$ is shown in Fig. 2b. Four bands can be seen at 1073, 1010, 953 and 925 cm^{-1} in the region of 1000 cm^{-1}. The bands centered at 3485 and 1630 cm^{-1} are probably due to v (O–H) and δ (H–O–H), respectively, of the water adsorbed in the surface of the sample.

3.3. Morphologies and structures of the products

Fig. 3 shows the SEM and TEM images of the as-synthesized $BiPO_4$ nano-cocoons at 200 °C for 1 h. The low-magnification SEM image shown in Fig. 3a displays that the sample is composed of a large scale of $BiPO_4$. Careful observation reveals that the size of the nano-cocoons typically ranges from 100 to 150 nm, as shown in Fig. 3b. The TEM image (Fig. 3c) shows that nano-cocoons exhibit relatively good dispersion. The corresponding discrete SAED spots (Fig. 3d) show that it is a well-crystallized single crystal, and all the spots can be indexed to hexagonal phase $BiPO_4$.

The morphology and size of the as-obtained monoclinic phase $BiPO_4$ at 200 °C for 3 h are observed by FESEM in Fig. 4a, which shows that the product consists of nanorods with diameters of 50–150 nm, lengths of 0.5–1.0 μm and an aspect ratio of 4–20. The high-magnification SEM image exhibits uniform column-like morphology with explicitly cut edges and a typical rectangular cross-section (Fig. 4b). The SAED pattern (inset of Fig. 4c) recorded on an individual $BiPO_4$ nanorod reveals the single-crystalline

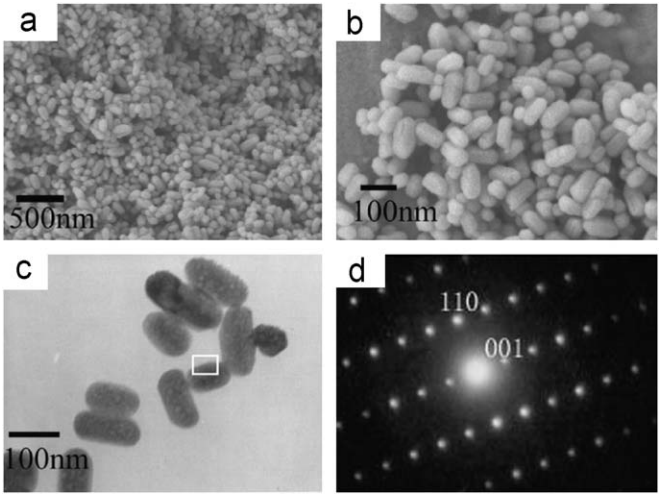

Fig. 3. Typical SEM and TEM images of the obtained $BiPO_4$ products at 200 °C for 1 h. (a) Low-magnification FE-SEM image of nano-cocoons; (b) high-magnification FE-SEM image of nano-cocoons; (c) TEM image of nano-cocoons; (d) the corresponding SAED pattern taken from the area labeled by rectangle in (c).

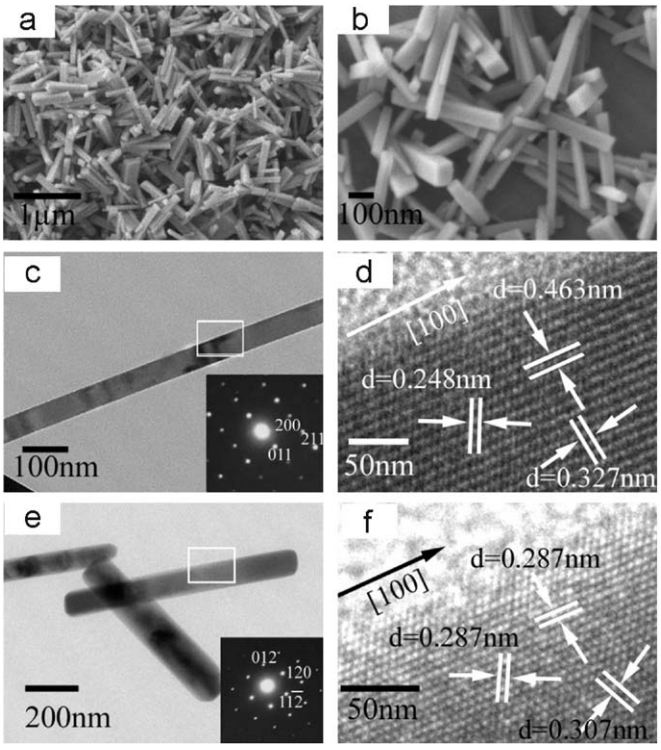

Fig. 4. Typical SEM and TEM images of the obtained $BiPO_4$ products at 200 °C for 3 h. (a) Low-magnification FE-SEM images of the nanorods; (b) high-magnification FE-SEM images of the products; (c) the high-magnification TEM of a nanorod; (d) HRTEM image taken from the area labeled by rectangle in (c); (e) the high-magnification TEM of another nanorod; (f) HRTEM image taken from the area labeled by rectangle in (e). The insets show the corresponding SAED patterns.

nature of the nanorod. Corresponding to the rectangular region in the individual nanorod in Fig. 4c, three interplanar spacings in various directions (0.248, 0.327 and 0.463 nm) are detected from the legible lattice fringes (Fig. 4d), corresponding to those of the (211), (200) and (011) planes of the monoclinic $BiPO_4$, respectively, revealing the growth direction of the $BiPO_4$ nanorods parallel to the (011) planes. The HRTEM image (Fig. 4f) of the rectangular region of another nanorod shows that the sample is structurally uniform with an interplanar spacing of about 0.307, 0.287 and 0.287 nm, which correspond to the (120), (012) and $(11\bar{2})$ lattice spacing of monoclinic $BiPO_4$ recorded on the SAED pattern (inset of Fig. 4e), respectively, revealing the growth direction of the $BiPO_4$ nanorods parallel to the (012) planes. $BiPO_4$ nanorods have a growth direction simultaneously parallel to the (011) planes and (012) planes, which exclusively indicates the growth direction of the $BiPO_4$ nanorods is the [100].

3.4. Evolution from hexagonal phase $BiPO_4$ to monoclinic phase $BiPO_4$

In order to understand the growth process of monoclinic phase $BiPO_4$ column-like nanorods, solvothermal synthesis was carried out for intermediate time. The product obtained at 200 °C for 1 h (Fig. 1a1) was hexagonal phase $BiPO_4$. The XRD the products for 1.5 h were similar to the data of the products for 1 h. Fig. 5a shows the XRD pattern of samples synthesized after reactions for 2 h. It can be seen that some characteristic peaks of monoclinic phase $BiPO_4$, with weak intensity, appeared on the XRD pattern. The characteristic peaks of monoclinic phase $BiPO_4$ were largely intensified, and those of hexagonal phase $BiPO_4$ were weakened as the reaction time was increased to 2.5 h (Fig. 5b). The peaks of hexagonal phase $BiPO_4$ eventually disappeared on the XRD pattern of products obtained at 200 °C for 3 h (Fig. 1a2). Corresponding to the above phase evolution, the time-dependent crystal morphology of the samples was reported in Fig. 5c and d. Fig. 5c shows the TEM image of the $BiPO_4$ nano-cocoons prepared at 200 °C for 2 h, which is similar to the products obtained at 200 °C for 1 h (Fig. 3c). The product synthesized at 200 °C for 2.5 h was composed of nano-cocoons and nanorods, as shown in Fig. 5d. Further increasing the reaction time to 3 h, column-like nanorods with explicitly cut edges were obtained (Fig. 4a). This evolution can be reasonably elucidated as follows: At first, a part of hexagonal phase $BiPO_4$ transformed to monoclinic phase $BiPO_4$, as shown in Fig. 5a. The phase transformation of $BiPO_4$ led to the

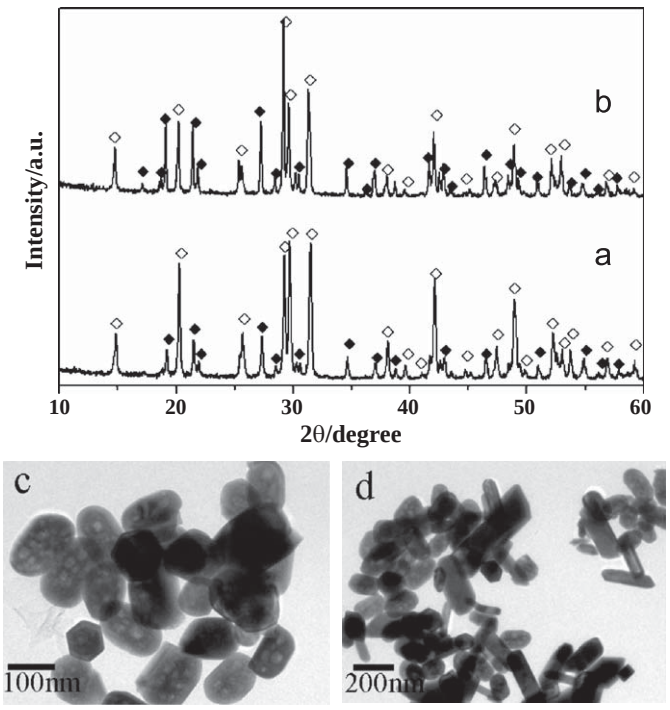

Fig. 5. XRD patterns of the products prepared at 200 °C for (a) 2 h and (b) 2.5 h; FE-SEM images of the products prepared at 200 °C for (c) 2 h and (d) 2.5 h. (◇: hexagonal phase $BiPO_4$; ♦: monoclinic phase $BiPO_4$.)

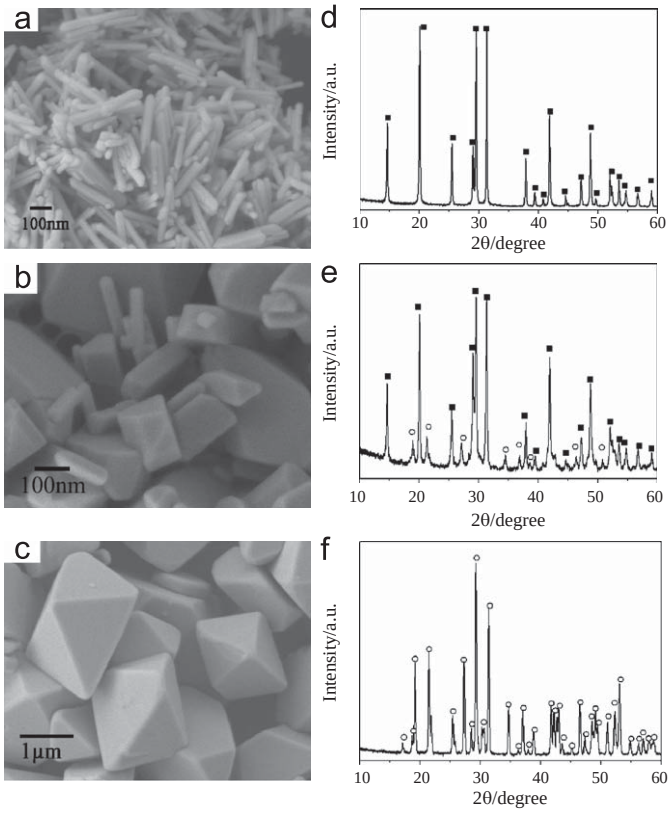

Fig. 6. SEM images of the products by hydrothermal method at 160 °C for (a) 1 h, (b) 2.5 h and (c) 12 h. The corresponding XRD patterns are shown in (d), (e) and (f). (■: hexagonal phase $BiPO_4$; ◦: monoclinic phase $BiPO_4$.)

change of intrinsic microstructure of the crystal. So, when the time was increased to 2.5 h, the phase transformation induced the morphology change. As seen in Fig. 5d, a part of hexagonal phase nano-cocoons transformed into monoclinic phase $BiPO_4$ nanorods. Therefore, the transformation of morphology reflects the intrinsic properties of the crystal.

The same phase transformation process occurred in the hydrothermal condition at 160 °C by varying the reaction time, accompanying with a morphology transformation from nanorods to octahedron-like microcrystals. The reason of choosing this temperature is that a high yield of BiPO4 octahedron-like microcrystals was formed under hydrothermal conditions. After hydrothermal treatment for 1 h, hexagonal phase nanorods were prepared, as shown in Fig. 6a and d. Increasing the reaction time to 2.5 h, the sample consisted of a mixture of hexagonal phase nanorods and monoclinic phase $BiPO_4$ irregular polyhedron structures (Fig. 6b and e). When the hydrothermal reaction time was extended to 12 h, monoclinic phase $BiPO_4$ octahedron-like microcrystals were obtained (Fig. 6c and f).

3.5. The influence of solvent

Further studies revealed that reaction time played an important role in the form of phase, while solvent had no effect on the phase. Whilst, in the present preparation process, it was found that the morphology and size of $BiPO_4$ were greatly affected by the ratios of the two components (glycerol and water) in the solvent. Herein, we used the products prepared at 200 °C for 3 h as a model system to demonstrate the morphology variation. We thus investigated this synthesis parameter in detail, and found that uniform monoclinic phase $BiPO_4$ nanorods were formed only in a

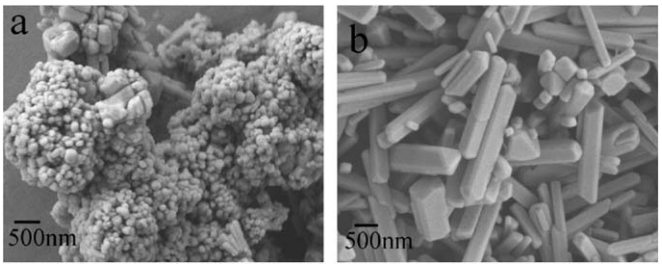

Fig. 7. SEM images of the products prepared in the presence of (a) 37 ml and (b) 15 ml glycerol at 200 °C for 3 h.

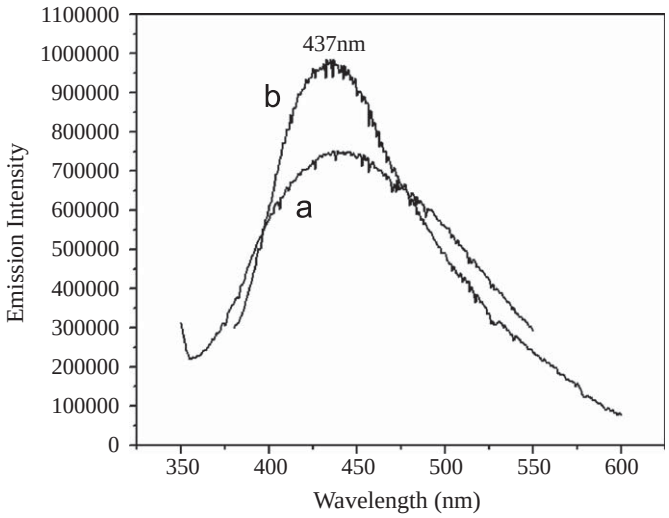

Fig. 8. PL spectra of as-prepared $BiPO_4$ products with different morphologies and phases: (a) hexagonal phase nano-cocoons; (b) monoclinic phase $BiPO_4$ nanorods.

suitable volume ratio range of between 1:1 and 2:1. When the ratio was above 2:1 or low 1:1, the morphology of obtained $BiPO_4$ was not uniform column-like structure with explicitly cut edges but irregular nanoparticles and rod-like structure, as shown in Fig. 7. The irregular nanoparticles (Fig. 7a) were obtained when the volume ratio was 5:1, while the rod-like structures with a diameter of 200–500 nm and an average length of 2 μm (Fig. 7b) were prepared when the volume ratio was 1:2. The experiment results showed that the appropriate amount of glycerol was vital for the formation of $BiPO_4$ column-like nanorods. As we know, the physical and chemical properties of the solvent can influence the solubility, reactivity, and diffusion behavior of the regents and the intermediate. As high viscosity solvent, glycerol with different amounts led to different diffusion rate of ions in the solution. So, higher volume ratio of glycerol to water was applied as solvent, crystalline growth was suppressed because of the low diffusion rate of ions in the solvent, and led to the formation of nanoparticles. On the other hand, lower volume ratio of glycerol to water led to the high diffusion rate of ions in the solution, as a result, rod-like structures were produced [13].

4. Optical properties

The fluorescence spectra of nano-cocoons and nanorods with $\lambda_{ex} = 360$ nm are shown in Fig. 8. Hexagonal phase $BiPO_4$ nano-cocoons and monoclinic phase $BiPO_4$ nanorods exhibit the same emission position at 437 nm; however, the emission intensity of monoclinic phase $BiPO_4$ nanorods is greater than that of hexagonal phase $BiPO_4$ nano-cocoons. The emission band observed from $BiPO_4$ is ascribed to the $^3P_1$–$^1S_0$ transitions [14].

Is the difference of the emission intensity due to the morphology or phase? To investigate the reason, the contradistinctive experiment was carried out under hydrothermal condition. It indicates that the emission intensity of hexagonal phase $BiPO_4$ nanorods is greater than that of monoclinic phase $BiPO_4$ octahedron-like microcystals. This suggests that the phase is not the main factor leading to the difference of emission intensity. It is thought that the difference of the emission intensity likely depends on their morphological variation. The fluorescence spectra clearly suggest that $BiPO_4$ is a reasonably luminescent material and probably this property can be exploited for possible future applications.

5. Conclusion

In summary, $BiPO_4$ hexagonal phase nano-cocoons and monoclinic phase $BiPO_4$ nanorods were selectively synthesized by solvothermal method. By varying the reaction time from 1 to 3 h at 200 °C, the evolution from hexagonal phase nano-cocoons to monoclinic phase nanorods was realized. In the hydrothermal condition at 160 °C, the similar phase transformation from hexagonal phase $BiPO_4$ to monoclinic phase $BiPO_4$ was also observed, accompanying with a morphology transformation from nanorods to octahedron-like microcrystals. The volume ratio of glycerol to water in the solvothermal condition had a great impact on the shapes of products. Moreover, the fluorescence spectra of hexagonal phase $BiPO_4$ nano-cocoons and monoclinic phase $BiPO_4$ nanorods were also studied.

Acknowledgments

We appreciated the financial support from the 973 Project of China (no. 2005CB623601), the National Natural Science Foundation of China (no. 20431020) and the China Postdoctoral Science Foundation (200801236).

References

[1] T.S. Chang, L. Guijia, Ch.H. Shin, Y.K. Lee, S.S. Yun, Catal. Lett. 68 (2000) 229–234.
[2] M. Ruwet, S. Ceckiewicz, B. Delmon, Ind. Eng. Chem. Res. 26 (1987) 1981–1983.
[3] K. Iitaka, Y. Tani, Y. Umezawa, Anal. Chim. Acta 338 (1997) 77–87.
[4] S. Kalaiselvan, R.K. Jeevanram, J. Radioanal. Nucl. Chem. 240 (1999) 277–279.
[5] Z. Holgye, J. Radioanal. Nucl. Chem. 227 (1998) 127–128.
[6] M.M. Charyulu, K.V. Chetty, D.G. Phal, V. Sagar, D.M. Naronha, S.M. Pawar, R. Swarup, V.V. Ramakrishna, V. Venugopal, J. Radioanal. Nucl. Chem. 251 (2002) 153–154.
[7] T. Jermoumi, M. Hafid, M. Et-tabirou, M. Taibi, H. ElQadim, N. Toreis, Mater. Sci. Eng. B 85 (2001) 28–33.
[8] M. Elmoudane, M. Et-tabirou, M. Hafid, Mater. Res. Bull. 35 (2000) 279–287.
[9] M.Y. Guan, J.H. Sun, F.F. Tao, Z. Xu, Cryst. Growth Des. 8 (2008) 2694–2697.
[10] J. Geng, W.H. Hou, Y.N. Lv, J.J. Zhu, H.Y. Chen, Inorg. Chem. 44 (2005) 8503–8509.
[11] Y.F. Lin, H.W. Chang, S.Y. Lu, C.W. Liu, J. Phys. Chem. C 111 (2007) 18538–18544.
[12] B. Romero, S. Bruque, M.A.G. Aranda, J.E. Iglesias, Inorg. Chem. 33 (1994) 1869–1874.
[13] S. Yin, M. Shinozaki, T. Sato, J. Lumin. 126 (2007) 427–433.
[14] A. Wolfert, E.W.J.L. Oomen, G. Blasse, J. Solid. State. Chem. 59 (1985) 280–290.